X-Ray Observations of the Isolated Black Hole Candidate OGLE-2011-BLG-0462 and Other Collapsed Objects Discovered through Gravitational Microlensing

S. Mereghetti[1] , L. Sidoli[1] , G. Ponti[2,3] , and A. Treves[2,4]
[1] INAF, Istituto di Astrofisica Spaziale e Fisica Cosmica, via A. Corti 12, I-20133 Milano, Italy; sandro.mereghetti@inaf.it
[2] INAF, Osservatorio Astronomico di Brera, via E. Bianchi 46, I-23807 Merate (LC), Italy
[3] Max-Planck-Institut für extraterrestrische Physik, Giessenbachstrasse, D-85748, Garching, Germany
[4] Universitá dell'Insubria, via Valleggio 11, I-22100 Como, Italy

Abstract

Isolated black holes and neutron stars can be revealed through the observation of long-duration gravitational microlensing events. A few candidates have been found in surveys of stars in the direction of the Galactic bulge. Recently, thanks to the addition of astrometric information at milliarcsecond level, it has been possible to reduce the uncertainties in the masses and distances for some of these "dark" gravitational lenses and select the most promising candidates. These isolated compact objects might emit X-rays powered by accretion from the interstellar medium. Using data of the Chandra, XMM-Newton, and INTEGRAL satellites, we searched for X-ray emission in the isolated black hole candidate OGLE-2011-BLG-0462, and in several other putative collapsed objects found with gravitational microlensing. OGLE-2011-BLG-0462 has been recently interpreted as a $7.1\,M_\odot$ black hole at a distance of 1.6 kpc, although a different group obtained a mass range (1.6–$4.4\,M_\odot$) that cannot exclude a massive neutron star. We have derived upper limits on the flux from OGLE-2011-BLG-0462 of 9×10^{-15} erg cm^{-2} s^{-1} in the 0.5–7 keV range and $\sim 2 \times 10^{-12}$ erg cm^{-2} s^{-1} in the 17–60 keV range. The implied X-ray luminosity is consistent with the small radiative efficiency expected for a black hole and disfavors a neutron star interpretation. Limits down to a factor of about five lower are obtained for the soft X-ray flux of other candidates, but their interpretation is affected by larger uncertainties in the masses, distances, and spatial velocities.

1. Introduction

Our galaxy is thought to contain of the order of 10^7–10^9 black holes (BHs), but only a few tens have been discovered so far in X-ray binaries (e.g., Corral-Santana et al. 2016). In fact, X-ray emission powered by accretion of matter from the binary companion star allows us to select candidates, which can be eventually confirmed as BHs by subsequent dynamical mass measurements. The presence of BHs has been claimed also in a few noninteracting binaries, based on radial velocity measurements of their companions (Liu et al. 2019; Thompson et al. 2019; Gomez & Grindlay 2021), but their true BH nature is debated (see, e.g., van den Heuvel & Tauris 2020; El-Badry & Quataert 2021, and references therein). A significant number of the BHs in the Galaxy should be isolated, either because they originated from single stars or because the binary in which they formed was disrupted by the natal supernova kick. In principle, such isolated BHs can be detected if they accrete matter from the interstellar medium (ISM; e.g., Shvartsman 1971; Ipser & Price 1982; Campana & Pardi 1993; Agol & Kamionkowski 2002), as it was also proposed for isolated neutron stars (Ostriker et al. 1970). However, several searches for isolated neutron stars (NSs) and BHs fed by accretion from the interstellar medium gave negative results (Stocke et al. 1995; Schwope et al. 1999; Chisholm et al. 2003; Muno et al. 2006), despite the initially optimistic estimates on the number of detectable objects (Treves & Colpi 1991; Blaes & Madau 1993).

Isolated BHs can also be detected through gravitational microlensing, when they pass in front of background stars (e.g., Paczynski 1986). Several long-duration microlensing events found in surveys targeted to stars in the Galactic bulge should be due to BHs, because the relative rarity of these objects is compensated by their large cross section. For most microlensing events only the crossing time of the Einstein radius can be measured. This timescale depends not only on the lens mass, but also on the relative velocities and distances of the lens and the lensed star. Therefore, on the basis of the sole crossing time, it is not possible to determine the individual values of these parameters. More information on the mass of the lens can be obtained in sufficiently long events, in which the effects caused by the nonlinear motion of the Earth can be detected in the light curve of the magnified star (Gould 1992). The first BH candidates selected with this method were reported by Bennett et al. (2002) and Mao et al. (2002). Note that, despite the "parallax microlensing" name of this phenomenon, it involves only photometric observations to measure the time-dependent deviations of the source magnification from the light curve expected with a simple model based on linear motions of the observer, lens, and lensed star. Due to the intrinsic degeneracy between the parameters that characterize parallax microlensing (in particular the one between lens mass and relative velocities) the masses derived in this way are subject to large uncertainties. This problem has usually been tackled by statistical analysis based on our best knowledge of the distributions of masses, positions, and velocities of the lens and of the lensed star (Agol et al. 2002). The nature of the lens (i.e., BH, NS, white dwarf, normal star) can thus be assessed in probabilistic terms.

A step forward to reduce such a degeneracy can be done if also the deviations in the apparent position of the magnified star caused by the gravitational lens are detected. This requires very accurate astrometric measurements at the milliarcsecond level. Recently, using this "astrometric microlensing" method, Sahu et al. (2022) derived a mass of $7.1 \pm 1.3 \, M_\odot$ and distance of 1.58 ± 0.18 kpc for the lens object in OGLE-2011-BLG-0462. Based on the lack of detectable light from the lens, these authors concluded that this is the first unambiguous detection of an isolated stellar-mass BH. Somewhat different results have been reported for the same event by Lam et al. (2022), who inferred a lens mass in the range 1.6–4.4 $M_\odot$, which leaves open the possibility that OGLE-2011-BLG-0462 could be an isolated NS.

X-ray observations of the compact objects found with gravitational microlensing can provide useful constraints on the physics of accretion. This is possibly the only way to derive information on accretion of the ISM onto isolated compact objects of stellar mass. A systematic comparative study between microlensing events and ROSAT sources was presented by Sartore & Treves (2012), finding no meaningful matching. Up to now, deep searches for X-ray emission have been reported only for MACHO-96-BLG-5 (Maeda et al. 2005; Nucita et al. 2006). The negative results imply accretion on the putative BH at a rate lower than $\sim 10^{-9}$ of the Eddington value.

Here we report on new and archival Chandra observations of the isolated BH candidate OGLE-2011-BLG-0462.[5] We also carried out a search for X-ray emission using all the available Chandra and XMM-Newton archival data for several other gravitational microlensing sources proposed, with different levels of confidence, as BH and NS candidates. To our knowledge, only the results for MACHO-98-BLG-5 have been previously reported in the literature. All the considered targets are briefly described in Section 2 while the data analysis and results are given in Section 3. The implications for the physics of accretion and future prospects are discussed in Sections 4 and 5.

2. Candidate BHs and NSs Found with Gravitational Microlensing

2.1. OGLE-2011-BLG-0462

OGLE-2011-BLG-0462 (also known as MOA-2011-BLG-191) is probably the most extensively studied BH candidate found through astrometric microlensing. Combining numerous data sets, including accurate astrometry carried out with the Hubble Space Telescope, Sahu et al. (2022) derived a lens mass $M_L = 7.1 \pm 1.3 \, M_\odot$. They also obtained stringent limits on the lens luminosity that rule out a nondegenerate star. These authors could exclude the possibility that the lens is a close[6] binary system, thus concluding that it is an isolated BH. The derived value of the lens distance is $D_L = 1.58 \pm 0.18$ kpc, only slightly dependent on the distance of the lensed star, and the lens transverse velocity is $V_T \sim 45$ km s^{-1}. They also noted that the region surrounding the lens is affected by severe differential extinction, which may indicate that locally the density of the ISM is large.

This microlensing event was studied also by Lam et al. (2022) who confirmed the dark nature of the lens. However, depending on the relative weights given to the astrometric and photometric data used in the fits, these authors found two solutions leading to different values for the lens mass, distance, and velocity (see Table 1). While one solution gives $M_L = 3.79^{+0.62}_{-0.57} \, M_\odot$, hence a high probability for a BH, the other one gives $M_L = 2.15^{+0.67}_{-0.54} \, M_\odot$, corresponding to comparable NS and BH probabilities. In both solutions, the transverse velocity of the lens ($V_T < 25$ km s^{-1}) is smaller than that obtained by Sahu et al. (2022).

2.2. MACHO-99-BLG-22

MACHO-99-BLG-22 (also known as OGLE-1999-BUL-32) was first pointed out as a possible BH by Mao et al. (2002), on the basis of a small parallax microlensing effect. The derived lens mass depends on the lens and source distances. For example, $M_L \sim 13 \, M_\odot$ for a source at the Galactic center distance of 8 kpc and a midway lens. The high likelihood of a BH nature was supported by a Bayesian statistical analysis that considered the mass functions of the disk and bulge stars (Agol et al. 2002). Poindexter et al. (2005) made a systematic analysis of 22 parallax microlensing events, taking into account various subtle effects that can lead to degenerate solutions and using a likelihood analysis to derive the masses. MACHO-99-BLG-22 was found to be the strongest BH candidate (78% probability) in their sample. In the following, we adopt their most likely values of $M_L \sim 7.5 \, M_\odot$ and $D_L \sim 4.8$ kpc.

2.3. MACHO-96-BLG-5

MACHO-96-BLG-5 is one of the two massive ($\sim 6 \, M_\odot$) and dark ($L < 1 \, L_\odot$) lenses found in an analysis of the longest microlensing events in the MACHO survey (Bennett et al. 2002). The lens mass–distance relation, assuming a source at the bulge distance of 8 kpc, gives most likely values in the ranges $M_L \sim 3$–16 $M_\odot$ and $D_L \sim 0.5$–2.2 kpc. The subsequent analysis of Poindexter et al. (2005) found a somewhat reduced probability of only 37% for a BH nature. A recent analysis of deep optical and near-infrared observations has strongly reduced the possible parameter space for a non-BH lens in MACHO-96-BLG-5 (Abdurrahman et al. 2021).

A 10 ks long observation of MACHO-96-BLG-5 was carried out with the Chandra ACIS-S instrument, but no X-rays were detected (Maeda et al. 2005), with a 99% confidence level upper limits on the 0.3–8 keV absorbed flux of $\sim 5 \times 10^{-15}$ erg cm^{-2} s^{-1}. Also a much longer (100 ks) observation with XMM-Newton could not detect any X-ray emission (Nucita et al. 2006) and provided slightly worse upper limits.

2.4. MACHO-98-BLG-6

MACHO-98-BLG-6 is the second BH candidate proposed by Bennett et al. (2002). With the assumption that the magnified star is at 8 kpc, Soto et al. (2007) derived $M_L = 6^{+9}_{-4} \, M_\odot$ and a distance $D_L = 1.9$ kpc. However, according to the analysis of Poindexter et al. (2005) MACHO-98-BLG-6 has a very small probability of being a BH (2%).

2.5. OGLE-2011-BLG-0310

OGLE-2011-BLG-0310 (also known as MOA-2011-BLG-332) is one of the five microlensing events for which an astrometric study has been carried out by Lam et al. (2022). However, these authors found an astrometric signal consistent with zero. According to their analysis, OGLE-2011-BLG-0310

---

[5] Our results supersede the limits quoted in Lam et al. (2022), which were obtained from a simple inspection of X-ray catalogs.
[6] A wide binary could not be excluded.

Table 1
Isolated BH and NS Candidates Found with Microlensing

Source	Mass $(M_\odot)$	Distance (kpc)	Comments	References
OGLE-2011-BLG-0462	7.1 ± 1.3	1.58 ± 0.18	$V_T = 45$ km s^{-1}	[S22]
	$3.79^{+0.62}_{-0.57}$	[1.47 − 1.92]	$V_T = 21$–27 km s^{-1}, 100% BH	[L22]
	$2.12^{+0.67}_{-0.54}$	[0.70 − 1.30]	$V_T = 2$–12 km s^{-1}, 44%, BH, 50% NS, 6% WD	[L22]
MACHO-99-BLG-22	7.5	4.8	78% BH, 7% NS, 4% WD	[M02,P05]
MACHO-96-BLG-5	6^{+10}_{-3}	$1.3^{+0.9}_{-0.8}$	37% BH, 14% NS, 19% WD	[B02,P05]
MACHO-98-BLG-6	6^{+9}_{-4}	1.9	2% BH, 13% NS, 26% WD	[B02,P05,S07]
OGLE-2011-BLG-0310	$0.78^{+0.71}_{-0.39}$	$4.3^{+1.9}_{-1.6}$	5% BH, 22% NS, 65% WD	[L22]
OGLE3-ULENS-PAR-01	$1.0^{+1.8}_{-0.7}$	$1.3^{+1.1}_{-0.7}$		[W16]
OGLE3-ULENS-PAR-02	$8.7^{+8.1}_{-4.7}$	$1.8^{+1.1}_{-0.8}$		[W16]
	$9.3^{+8.7}_{-4.3}$	$2.4^{+1.1}_{-1.0}$		
OGLE3-ULENS-PAR-05	$3.3^{+2.7}_{-1.5}$	$2.9^{+1.1}_{-0.9}$		[W16]
	$4.8^{+4.0}_{-2.5}$	$1.8^{+1.2}_{-0.7}$		
MOA-2009-BLG-260	$1.37^{+2.72}_{-1.16}$	$5.0^{+1.7}_{-1.3}$	14% BH, 44% NS, 38% WD	[L22]
OGLE-00-BUL-43	$2.9^{+6.1}_{-1.9}$	0.5	for disk lensed source	[S07]
	$2^{+6}_{-1.5}$	0.8	for bulge lensed source	

Note.

References. [S22] Sahu et al. (2022), [L22] Lam et al. (2022), [W16] Wyrzykowski et al. (2016), [P05] Poindexter et al. (2005), [B02] Bennett et al. (2002), [S07] Soto et al. (2007), [M02] Mao et al. (2002).

is most likely a white dwarf (65% probability) or an NS (22%) with mass of $0.78^{+2.98}_{-0.68}\,M_\odot$.

2.6. OGLE3-ULENS-PAR-01, PAR-02, and PAR-05

Wyrzykowski et al. (2016) made an extensive search for BH, NS, and white dwarf candidates in the OGLE-III database. They found 13 out of 59 parallax microlensing events consistent with a compact object lens. Their masses and distances were estimated assuming standard proper motions for stars in the Galaxy. Although it cannot be excluded that some of them are main-sequence stars in the disk that move in parallel with bulge sources giving very small relative proper motions, a few interesting candidates were selected. OGLE3-ULENS-PAR-02 and OGLE3-ULENS-PAR-05 are those with the highest estimated masses, consistent with being BHs. Both of them have two possible solutions yielding slightly different parameters (see Table 1).

2.7. MOA-2009-BLG-260

MOA-2009-BLG-260 is an astrometric parallax event with mass $M_L = 1.37^{+0.74}_{-0.60}$ (Lam et al. 2022), most likely consisting of an NS (44% probability). No Chandra or XMM-Newton observations of its position are available.

2.8. OGLE-00-BUL-43

Soto et al. (2007) performed spectroscopy of 16 microlensing events to add radial velocity information and determine spectral types, and estimated lens masses based on a model of the Galaxy. OGLE-00-BUL-43 was found as a possible BH candidate, but no Chandra or XMM-Newton observations are available.

3. X-Ray Data Analysis and Results

Chandra observations are available for six of the microlensing events listed in Table 1: OGLE-2011-BLG-0462, MACHO-99-BLG-22, MACHO-98-BLG-5, OGLE-2011-BLG-0310,

OGLE3-ULENS-PAR-05, and OGLE3-ULENS-PAR-01. Four of them have also XMM-Newton observations, but these data have a worse sensitivity compared to the Chandra ones and will not be considered in the following. We report the results obtained with XMM-Newton only for the two sources not observed with Chandra: MACHO-98-BLG-6 and OGLE3-ULENS-PAR-02. A log of the observations used in our analysis is given in Table 2.

3.1. Chandra

Chandra data reprocessing and analysis were performed with standard procedures using the most recent version of the Chandra Interactive Analysis of Observation (CIAO 4.14) and CALDB (4.9.6). Images and exposure maps were produced using FLUXIMAGE in the energy range 0.5–7.0 keV. The script SRCFLUX was used to estimate the radii of the circular regions enclosing 90% of the point-spread function at 1.0 keV. Such radii range from 0″.9 on-axis to 9″ for the most off-axis sources. The background for each observation was estimated using annular regions centered on the source positions, with inner and outer radii of one and five times the source extraction radius. These source-free background regions contain zero or, at most, a few counts. The effective exposures used for the flux computation take into account the off-axis positions of the sources and have been computed taking the average exposure time inside the source extraction circle.

No X-ray sources were detected at the sky positions of the microlensing events. Given the small number of detected counts, the upper limits on the count rates (95% c.l.) were computed following Kraft et al. (1991). These limits were then converted to fluxes using the appropriate calibration files for each source and observation. Such conversions depend on the assumed spectral shape and absorption. We used a power-law spectrum with photon index of 2 and interstellar medium abundances from Wilms et al. (2000). The total hydrogen column densities in the directions of our targets are in the range $[2\text{–}6] \times 10^{21}$ cm^{-2} (HI4PI Collaboration et al. 2016). Given that the lenses are at intermediate distances between us and the Galactic bulge, these values can be regarded as upper limits.

Table 2
X-Ray Observations of Microlensing Events

Source	Satellite	ObsID	Date	Instrument	Duration (ks)	Effective Exposure (ks)	Off-axis Angle (′)
OGLE-2011-BLG-0462	Chandra	8764	2008-05-13	ACIS-I (VF)	2.15	1.92	8.8
	Chandra	13540	2011-11-01	ACIS-I (VF)	1.95	1.83	5.1
	Chandra	21628	2019-07-29	ACIS-I (VF)	1.89	1.74	6.6
	Chandra	23951	2022-06-02	ACIS-I (VF)	5.29	4.84	5.1
MACHO-99-BLG-22	Chandra	3818	2003-08-01	ACIS-S (VF)	9.7	9.36	0.0
MACHO-96-BLG-5	Chandra	3789	2003-02-18	ACIS-S (F)	9.83	9.83	0.0
	Chandra	14677	2013-10-03	ACIS-I (F)	1.0	0.95	7.6
MACHO-98-BLG-6	XMM	0782770201	2016-09-03	EPIC MOS1	40	30.7	4.3
OGLE-2011-BLG-0310	Chandra	13542	2011-11-01	ACIS-I (VF)	1.95	1.864	8.7
	Chandra	13564	2011-11-01	ACIS-I (VF)	1.95	1.785	10
	Chandra	13565	2011-11-01	ACIS-I (VF)	1.95	1.744	5.9
	Chandra	23957	2021-03-18	ACIS-I (VF)	5.1	4.52	7.5
OGLE3-ULENS-PAR-01	Chandra	7541	2007-10-23	HRC-I	1.19	1.17	13.8
OGLE3-ULENS-PAR-02	XMM	0782770201	2016-09-03	EPIC pn	35	32	0.0
OGLE3-ULENS-PAR-05	Chandra	19723	2018-05-10	ACIS-I (VF)	19.8	19.8	0.0

Note. VF and F in column (5) indicate very faint and faint mode, respectively.

Table 3
X-Ray Upper Limits (95% c.l.)

Source	ObsID	Count Rate (count s^{-1})	Observed Flux 0.5–7 keV (erg cm^{-2} s^{-1})	$N_{\rm H}$ (cm^{-2})	Unabsorbed Flux 0.5–7.0 keV (erg cm^{-2} s^{-1})	Unabsorbed Flux 0.1–100 keV (erg cm^{-2} s^{-1})
OGLE-2011-BLG-0462	8764	<0.0016	$<2.20 \times 10^{-14}$	10^{21}	$<2.57 \times 10^{-14}$	$<6.76 \times 10^{-14}$
	13540	<0.0016	$<1.93 \times 10^{-14}$		$<2.25 \times 10^{-14}$	$<5.92 \times 10^{-14}$
	21628	<0.0017	$<3.16 \times 10^{-14}$		$<3.69 \times 10^{-14}$	$<9.71 \times 10^{-14}$
	23951	<0.00126	$<2.72 \times 10^{-14}$		$<3.17 \times 10^{-14}$	$<8.31 \times 10^{-14}$
	combined	<0.00051	$<8.6 \times 10^{-15}$		$<1.0 \times 10^{-14}$	$<2.6 \times 10^{-14}$
MACHO-99-BLG-22	3818	$<3.2 \times 10^{-4}$	$<1.99 \times 10^{-15}$	3×10^{21}	$<2.83 \times 10^{-15}$	$<7.43 \times 10^{-15}$
MACHO-96-BLG-5	3789	$<3.1 \times 10^{-4}$	$<1.86 \times 10^{-15}$	10^{21}	$<2.17 \times 10^{-15}$	$<5.71 \times 10^{-15}$
	14677	<0.0032	$<5.63 \times 10^{-14}$		$<6.57 \times 10^{-14}$	$<1.73 \times 10^{-13}$
MACHO-98-BLG-6	0782770201	$<9 \times 10^{-4}$	$<9.77 \times 10^{-15}$	10^{21}	$<1.14 \times 10^{-14}$	$<3.0 \times 10^{-14}$
OGLE-2011-BLG-0310	13542	<0.0031	$<4.37 \times 10^{-14}$	5×10^{21}	$<7.1 \times 10^{-14}$	$<1.9 \times 10^{-13}$
	13564	<0.0032	$<4.97 \times 10^{-14}$		$<8.0 \times 10^{-14}$	$<2.1 \times 10^{-13}$
	13565	<0.0026	$<3.60 \times 10^{-14}$		$<5.8 \times 10^{-14}$	$<1.5 \times 10^{-13}$
	23957	<0.00066	$<1.42 \times 10^{-14}$		$<2.3 \times 10^{-14}$	$<6.0 \times 10^{-14}$
	combined	<0.0009	$<1.54 \times 10^{-14}$		$<2.5 \times 10^{-14}$	$<6.6 \times 10^{-14}$
OGLE3-ULENS-PAR-01	7541	<0.0178	$<4.37 \times 10^{-13}$	10^{21}	$<5.1 \times 10^{-13}$	$<1.3 \times 10^{-12}$
OGLE3-ULENS-PAR-02	0782770201	$<2.55 \times 10^{-3}$	$<6.08 \times 10^{-15}$	10^{21}	$<7.1 \times 10^{-15}$	$<1.9 \times 10^{-14}$
OGLE3-ULENS-PAR-05	19723	<0.00015	$<2.11 \times 10^{-15}$	2×10^{21}	$<2.76 \times 10^{-15}$	$<7.24 \times 10^{-15}$

Note. All count rates are in the energy range 0.5–7 keV, except Chandra HRC-I rates, which are in the energy range 0.1–10 keV, and XMM-Newton count rates (0.2–12 keV).

We inspected the run of extinction versus distance in the direction of each source derived by Green et al. (2019) and, based on the lens distance, we rescaled the total hydrogen column densities to obtain the $N_{\rm H}$ values listed in Table 3. These values were used to compute the unabsorbed fluxes. When HRC-I data were analyzed, the upper limit on the net count rate was estimated in the energy range 0.1–10 keV, but the fluxes have been converted to the 0.5–7 keV band. All the results are reported in Table 3.

3.2. XMM-Newton

An XMM-Newton observation was targeted at the event OGLE3-ULENS-PAR-02 in 2016 September. We used the data obtained with the EPIC pn camera that was operated in prime full window mode with the thin optical filter. XMM-Newton data were analyzed with the science analysis software (SAS) adopting standard procedures. A faint source (4XMM J 175723.4–284627 in the XMM-Newton Serendipitous Source Catalog; Webb et al. 2020) is detected at an angular distance of 6″6 from the position of OGLE3-ULENS-PAR-02. Its net count rate, measured using an extraction radius of 20″, is $(2.55 \pm 0.75) \times 10^{-3}$ counts s^{-1} in the 0.2–12 keV range. The error on its coordinates (0″98 statistical, 0″45 systematic, 1σ c.l.) is sufficiently small to exclude that this source is related to OGLE3-ULENS-PAR-02.

The instrument sensitivity at the position of the gravitational lens is reduced due to the presence of this nearby contaminating source. Therefore, we conservatively assume as an upper limit the count rate of 4XMM J 175723.4–284627. For a power-law spectrum with photon index of 2 and $N_H = 10^{21}$ cm^{-2} this
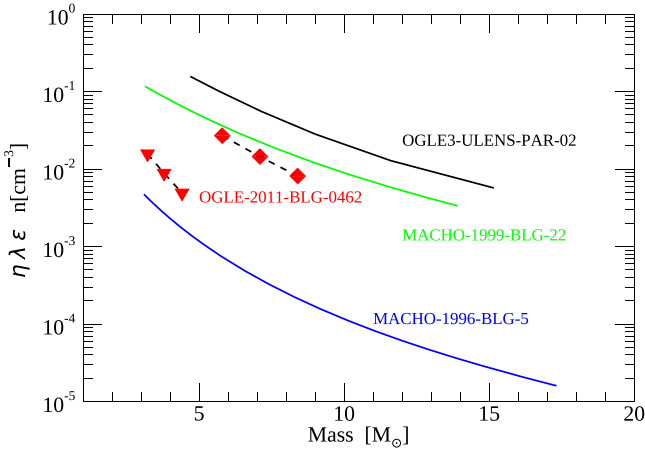
Figure 1. Constraints on the product of BH efficiency $\eta(\equiv L/\dot{M}c^2)$ and ISM density derived from the X-ray flux upper limits of OGLE-2011-BLG-0462 (red) and other BH candidates found with gravitational microlensing (see text for the definition of λ and ϵ). The red diamonds and triangles refer to the BH properties derived by Sahu et al. (2022) and Lam et al. (2022), respectively. The curves for the other BH candidates are derived using for each mass value the corresponding distance and transverse velocity as given by the microlensing relations.

count rate corresponds to an unabsorbed 0.2–12 keV flux of 1.1×10^{-14} erg cm^{-2} s^{-1} (or 7.1×10^{-15} erg cm^{-2} s^{-1} in the 0.5–7 keV range used above for Chandra).

The same XMM-Newton observation covers also the sky position of the event MACHO-98-BLG-6, lying about 4.'3 offset. For this event we analyzed the EPIC MOS data (effective exposure $T_{\text{exp}} = 30.7$ ks, MOS1), because its sky position lies very close to the gap between charged coupled devices in the pn camera, hampering a proper determination of the upper limit. We have measured a 95% upper limit to the count rate of 9.0×10^{-4} counts s^{-1} (0.2–12 keV), using the SAS script EUPPER. With the same assumptions on the spectrum used above, this translates into an upper limit to the unabsorbed flux of 1.78×10^{-14} erg cm^{-2} s^{-1} (1.14×10^{-14} erg cm^{-2} s^{-1}, 0.5–7 keV).

4. Discussion

The accretion-powered luminosity of an isolated compact star of mass M moving with velocity V in the interstellar medium of density n depends on the mass accretion rate $\dot{M}$, that, in the Bondi–Hoyle description, is given by

$$\dot{M} = 4\pi n m_p \frac{(GM)^2}{(V^2 + c_s^2)^{3/2}} \lambda \quad \text{g s}^{-1}. \tag{1}$$

Here G is the gravitational constant, m_p the proton mass, and c_s the sound speed, which we will neglect in the following because, for the most common phases of the ISM, it is much smaller than the typical space velocity of isolated NSs and BHs. The parameter λ accounts for the fact that not all the matter crossing the Bondi–Hoyle radius is accreted. As discussed in Tsuna et al. (2018), its value is subject to a large uncertainty. Therefore, we keep it as an explicit scaling factor in all the results given below and in Figure 1.

According to the analysis of Lam et al. (2022), there is a nonnegligible probability that OGLE-2011-BLG-0462 is an NS rather than a BH; also other objects listed in Table 1 are most

likely NSs. Therefore, in the following we discuss both the BH and NS case.

4.1. Black Hole

Sahu et al. (2022), derived for OGLE-2011-BLG-0462 a transverse velocity of 45 km s^{-1}. We can thus neglect c_s in Equation (1) and, with the 7.1 $M_\odot$ mass given by these authors, estimate an accretion rate of $2 \times 10^{11} n\lambda$ g s^{-1}. This is actually an upper limit because it does not take into account the unknown component of the velocity along the line of sight. Then, for the BH distance $d = 1.58$ kpc, the upper limit on the X-ray flux derived above, $F_X < 8.9 \times 10^{-15}$ erg cm^{-2} s^{-1}, implies a luminosity

$$L < \frac{F_X}{\epsilon} 4\pi d^2 = 2.7 \times 10^{30}/\epsilon \quad \text{erg s}^{-1}, \tag{2}$$

and an efficiency of conversion of gravitational energy to electromagnetic radiation

$$\eta \equiv L/(\dot{M}c^2) < \frac{0.015}{\epsilon\lambda} \left(\frac{n}{1 \text{ cm}^{-3}}\right)^{-1}, \tag{3}$$

where we introduced the factor ϵ to account for the fraction of accretion luminosity falling outside the observed X-ray band. Assuming that the luminosity is emitted in the 0.1–100 keV range with a power-law spectrum of photon index $\alpha = 2$, the 0.5–7 keV range used above corresponds to $\epsilon = F_{0.5-7}/F_{0.1-100} = 0.38$ ($\epsilon = 0.2/0.34$ for $\alpha = 1.5/2.5$).

Lam et al. (2022) found for the BH case a most likely mass of 3.8 $M_\odot$ and a transverse velocity in the range 21–27 km s^{-1}. The mass accretion rate has a strong dependence on the BH velocity. Thus, despite the smaller mass, the limit on η obtained using these values is more constraining than that derived above. This is shown in Figure 1, where the upper limit on the product $\eta\lambda\epsilon n$ is plotted as a function of the BH mass for both the Sahu et al. (2022) and Lam et al. (2022) parameters.

We plot in Figure 1 also the constraints obtained in a similar way from our upper limits on the X-ray fluxes of the other candidates of Table 1 that are likely to be BHs. To derive the limits for these sources, which, contrary to OGLE-2011-BLG-0462, do not have an astrometric parallax measurement, we took into account the distance dependence of the mass and transverse velocity. Our constraints for MACHO-96-BLG-5 agree with those derived by Maeda et al. (2005) using the same data. These constraints are below those of OGLE-2011-BLG-0462, but note that, besides having a large distance uncertainty, after the analysis of Poindexter et al. (2005) MACHO-96-BLG-5 is no more considered a strong BH candidate.
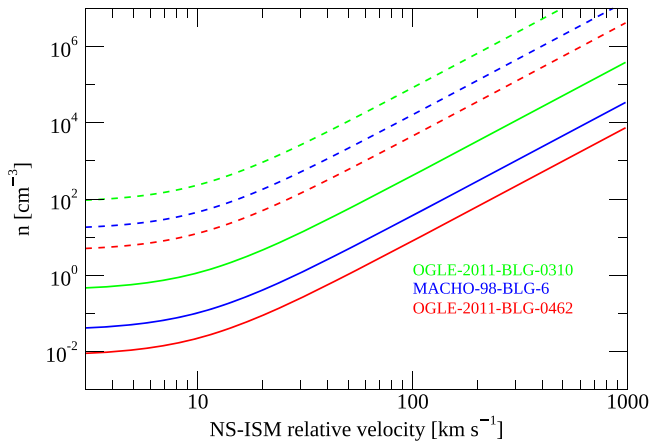
4.2. Neutron Star

The expected accretion luminosity for an NS of mass M_{NS} and radius R_{NS} is

$$L_{\text{NS}} = \frac{GM_{\text{NS}}}{R_{\text{NS}}}\dot{M} = \frac{(GM_{\text{NS}})^3}{R_{\text{NS}}V^3}4\pi m_p n\lambda, \tag{4}$$

which, for $M_{\text{NS}} = 1.4 M_\odot$ and $R_{\text{NS}} = 10$ km, gives a luminosity

$$L_{\text{NS}} = 1.3 \times 10^{32} \left(\frac{10 \text{ km s}^{-1}}{V}\right)^3 n\lambda \quad \text{erg s}^{-1}. \tag{5}$$

For the small distance (0.7–1.3 kpc at 99% c.l.) and transverse velocity (2–12 km s^{-1}) derived for OGLE-2011-BLG-0462 in

Figure 2. Constraints on the NS velocity and ISM density for candidate isolated NSs found with gravitational microlensing. A sound speed $c_s = 10$ km s^{-1} has been assumed. The regions above the solid lines are excluded by the upper limits on the soft X-ray flux obtained with Chandra, while those above the dashed lines are excluded by the INTEGRAL limits in the hard X-ray range (17–60 keV).
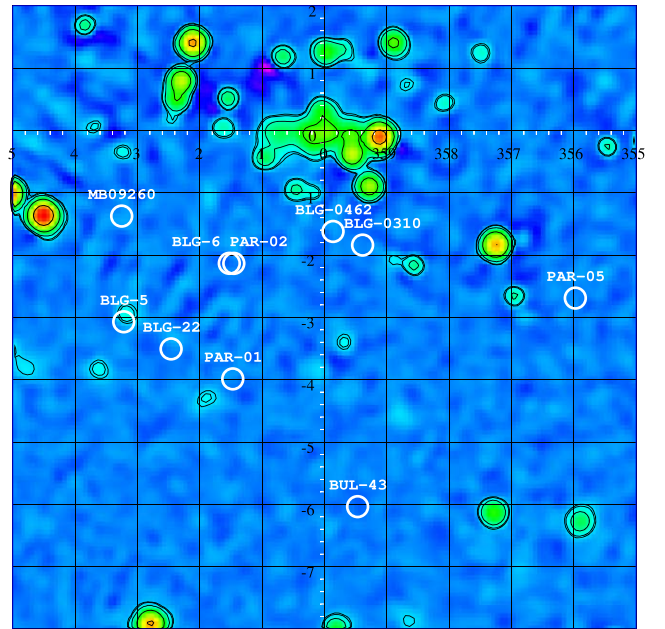

Figure 3. Image in the 17–60 keV range obtained with the INTEGRAL IBIS instrument (adapted from Krivonos et al. 2022). The image is in Galactic coordinates and covers a region of about 10×10 deg^2. The positions of the BH/NS candidates found with gravitational microlensing are indicated by circles with a radius of 10′. The source on the border of the MACHO-96-BLG-5 circle, IGR J18044−2739, is identified with a magnetic cataclysmic variable (Masetti et al. 2012). Its coordinates are incompatible with those of the microlens source.

the NS case (Lam et al. 2022), the resulting flux is in the broad range $F_X = [0.6 - 140] \times 10^{-12} n\lambda/d_{\mathrm{kpc}}^2$ erg cm^{-2} s^{-1}. This expected flux is close to, or higher than, the upper limit of $\sim 10^{-14}$ erg cm^{-2} s^{-1} derived above, thus possibly disfavoring an NS nature.

Taking booth λ and $d_{\mathrm{kpc}} \sim 1$, implies that the NS is in a low density ($n \lesssim 10^{-2}$ cm^{-3}) environment, but unfortunately, no strong conclusions can be drawn because the radial component of the NS is unknown. Isolated NS have relatively high space velocities. Hobbs et al. (2005) found that radio pulsars have a velocity distribution consistent with a Maxwellian with rms $\sigma = 265$ km s^{-1}, while a more recent analysis found that the sum of two Maxwellian distributions with $\sigma_1 = 128$ km s^{-1} and $\sigma_2 = 298$ km s^{-1} gives a better description of the pulsar velocity distribution (Igoshev 2020).

We show in Figure 2 how the upper limits on the X-ray flux we derived for the microlensing NS candidates translate into constraints on the ISM density as a function of their space velocities. For all the candidates we assumed $M_{\mathrm{NS}} = 1.4\,M_\odot$, $R_{\mathrm{NS}} = 10$ km, the best-fit distances given in Table 1, $\lambda = 1$, and an ISM sound speed of $c_s = 10$ km s^{-1}. For example, if OGLE-2011-BLG-0462 has a space velocity below 100 km s^{-1}, it cannot be in a region of the ISM with density higher than ~ 10 cm^{-3}. This excludes that OGLE-2011-BLG-0462 is either inside or within the envelope of a molecular cloud.

4.3. Limits in the Hard X-Ray Band

If these compact objects are in dense molecular clouds, their flux can be severely absorbed in the softest part of the energy range explored with Chandra and XMM-Newton. It is therefore interesting to search also for X-ray emission in the hard X-ray range, that is unaffected by interstellar absorption. All the microlensing events considered here are in the direction of the Galactic bulge, a region that has been extensively observed with the INTEGRAL satellite. The positions of the microlensing candidates are marked in Figure 3 on a sky map obtained with the INTEGRAL IBIS instrument (Ubertini et al. 2003) in the 17–60 keV energy range. This image has been derived by summing observations carried out from 2002 to 2017 and

corresponds to a total net exposure time of more than 13 millions of seconds (Krivonos et al. 2022). The resulting limiting sensitivity is $\sim 2 \times 10^{-12}$ erg cm^{-2} s^{-1}.

Since no hard X-ray sources are detected at the positions of the microlensing events, we used this flux value to derive the limits shown by the dashed lines in Figure 2. Although these limits are above those obtained in soft X-rays, they do not depend on the absorption and can be applied also for sources inside dense molecular clouds.

5. Conclusions

We derived upper limits on the X-ray flux from OGLE-2011-BLG-0462. This is currently the strongest BH candidate selected through astrometric gravitational microlensing (Sahu et al. 2022), although there is some tension in its parameters as derived by different groups and an NS nature cannot be completely excluded (Lam et al. 2022). Our limits are consistent with an accreting isolated BH with low radiative efficiency, as observed in quiescent X-ray binaries and in active galactic nuclei, and do not support an NS nature for the lens in OGLE-2011-BLG-0462. However, we cannot exclude the possibility of an NS in a relatively low density environment and/or with a space velocity much larger than the projected value obtained from the gravitational microlensing analysis.

Using Chandra, XMM-Newton and INTEGRAL data, we derived upper limits on the soft and hard X-ray fluxes also for several other candidate compact objects found with gravitational microlensing. The limits reported here are the best ones currently available for these objects, but the resulting constraints on the physical parameters governing the accretion process depend on several poorly known factors. Among these, a major role is played by the space velocity of the compact

object, since even a factor of two yields a difference of about one order of magnitude in the expected accretion rate. In fact, the relative positions of the limits plotted in Figure 1 are determined mainly by the different velocities of these objects.

Further observations will provide better estimates of the masses and distances of these candidate collapsed objects and possibly discriminate between BHs and NSs, but the radial velocity component of dark lenses cannot be directly measured. This problem will always affect the interpretation of X-ray observations of individual sources. However, many more isolated BHs and NSs will be discovered with microlensing surveys in the future. Thanks to the availability of a large sample of reliable candidates observed with high-sensitivity X-ray telescopes, it will be possible to perform statistical analysis exploiting our best knowledge of the distribution of spatial velocities, thus deriving meaningful constraints on the physics of accretion from the ISM onto isolated compact objects.

ORCID iDs

S. Mereghetti ⓘ https://orcid.org/0000-0003-3259-7801
L. Sidoli ⓘ https://orcid.org/0000-0001-9705-2883
G. Ponti ⓘ https://orcid.org/0000-0003-0293-3608
A. Treves ⓘ https://orcid.org/0000-0002-0653-6207

References

Abdurrahman, F. N., Stephens, H. F., & Lu, J. R. 2021, ApJ, 912, 146
Agol, E., & Kamionkowski, M. 2002, MNRAS, 334, 553
Agol, E., Kamionkowski, M., Koopmans, L. V. E., & Blandford, R. D. 2002, ApJL, 576, L131
Bennett, D. P., Becker, A. C., Quinn, J. L., et al. 2002, ApJ, 579, 639
Blaes, O., & Madau, P. 1993, ApJ, 403, 690
Campana, S., & Pardi, M. C. 1993, A&A, 277, 477
Chisholm, J. R., Dodelson, S., & Kolb, E. W. 2003, ApJ, 596, 437
Corral-Santana, J. M., Casares, J., Muñoz-Darias, T., et al. 2016, A&A, 587, A61
El-Badry, K., & Quataert, E. 2021, MNRAS, 502, 3436
Gomez, S., & Grindlay, J. E. 2021, ApJ, 913, 48
Gould, A. 1992, ApJ, 392, 442
Green, G. M., Schlafly, E., Zucker, C., Speagle, J. S., & Finkbeiner, D. 2019, ApJ, 887, 93
HI4PI Collaboration, Ben Bekhti, N., Flöer, L., et al. 2016, A&A, 594, A116
Hobbs, G., Lorimer, D. R., Lyne, A. G., & Kramer, M. 2005, MNRAS, 360, 974
Igoshev, A. P. 2020, MNRAS, 494, 3663
Ipser, J. R., & Price, R. H. 1982, ApJ, 255, 654
Kraft, R. P., Burrows, D. N., & Nousek, J. A. 1991, ApJ, 374, 344
Krivonos, R. A., Sazonov, S. Y., Kuznetsova, E. A., et al. 2022, MNRAS, 510, 4796
Lam, C. Y., Lu, J. R., Udalski, A., et al. 2022, ApJL, 933, L23
Liu, J., Zhang, H., Howard, A. W., et al. 2019, Natur, 575, 618
Maeda, Y., Kubota, A., Kobayashi, Y., et al. 2005, ApJL, 631, L65
Mao, S., Smith, M. C., Woźniak, P., et al. 2002, MNRAS, 329, 349
Masetti, N., Nucita, A. A., & Parisi, P. 2012, A&A, 544, A114
Muno, M. P., Bauer, F. E., Bandyopadhyay, R. M., & Wang, Q. D. 2006, ApJS, 165, 173
Nucita, A. A., De Paolis, F., Ingrosso, G., et al. 2006, ApJ, 651, 1092
Ostriker, J. P., Rees, M. J., & Silk, J. 1970, ApL, 6, 179
Paczynski, B. 1986, ApJ, 304, 1
Poindexter, S., Afonso, C., Bennett, D. P., et al. 2005, ApJ, 633, 914
Sahu, K. C., Anderson, J., Casertano, S., et al. 2022, ApJ, 933, 83
Sartore, N., & Treves, A. 2012, A&A, 539, A52
Schwope, A. D., Hasinger, G., Schwarz, R., Haberl, F., & Schmidt, M. 1999, A&A, 341, L51
Shvartsman, V. F. 1971, SvA, 15, 377
Soto, M., Minniti, D., & Rejkuba, M. 2007, A&A, 466, 157
Stocke, J. T., Wang, Q. D., Perlman, E. S., Donahue, M. E., & Schachter, J. F. 1995, AJ, 109, 1199
Thompson, T. A., Kochanek, C. S., Stanek, K. Z., et al. 2019, Sci, 366, 637
Treves, A., & Colpi, M. 1991, A&A, 241, 107
Tsuna, D., Kawanaka, N., & Totani, T. 2018, MNRAS, 477, 791
Ubertini, P., Lebrun, F., Di Cocco, G., et al. 2003, A&A, 411, L131
van den Heuvel, E. P. J., & Tauris, T. M. 2020, Science,, 368, eaba3282
Webb, N. A., Coriat, M., Traulsen, I., et al. 2020, A&A, 641, A136
Wilms, J., Allen, A., & McCray, R. 2000, ApJ, 542, 914
Wyrzykowski, Ł., Kostrzewa-Rutkowska, Z., & Skowron, J. 2016, MNRAS, 458, 3012